Kink Sum for Long-Memory Small Matrix Path Integral Dynamics

Nancy Makri*

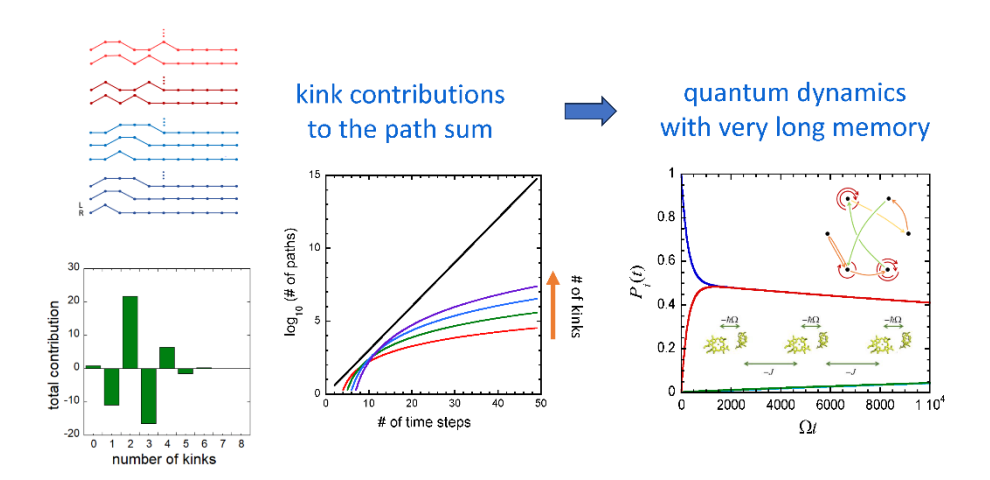
Departments of Chemistry and Physics, University of Illinois 505 S. Mathews Avenue, Urbana, IL 61801

Abstract

The small matrix decomposition of the real-time path integral (SMatPI) allows numerically exact and efficient propagation of the reduced density matrix (RDM) for system-bath Hamiltonians. Its high efficiency lies in the small size of the SMatPI matrices employed in the iterative algorithm, whose size is equal to that of the full RDM. By avoiding the storage and multiplication of large tensors, the SMatPI algorithm is applicable to multistate systems under a variety of conditions. The main computational effort is the evaluation of path sums within the entangled memory length to construct the SMatPI matrices. A number of methods are available for this task, each with its own favorable parameter regime, but calculations with strong system-bath coupling and long memory at low temperatures remain out of reach. The present paper evaluates the path sums by binning the paths (in forward time only) based on their amplitudes, which depend on the number and type of kinks they contain. The algorithm is very efficient, leading to a dramatic acceleration of path sums and significantly extending the accessible memory length in the most challenging regimes.

Author's email: nmakri@illinois.edu

TOC graphic:



1. Introduction

Quantum mechanical phenomena are ubiquitous and play a vital role in the dynamics of condensed phase processes. In addition, quantum effects can inform the design of novel materials for solar energy harvest and of architectures suitable for quantum information technology. The quest for novel technologies has spurred a renewed interest in the development of robust, efficient and accurate methods for simulating the quantum dynamics of large molecular aggregates and systems in condensed phase environments.

Numerically exact time-dependent wavefunction methods, most notably the multiconfiguration time-dependent Hartree (MCTDH) method¹⁻² and algorithms based on the density matrix renormalization group³⁻⁴ (DMRG) are suitable for small- to medium-sized molecules and systems with a linear topology. Simulating dynamical processes in liquids and biomolecules requires entirely different approaches that generally rely on various assumptions and approximations. Many methods utilize classical trajectories, which they either augment to capture quantum effects or combine with a quantum mechanical treatment for select degrees of freedom. When all degrees of freedom are treated on the same footing on a single Born-Oppenheimer potential surface, the linearized semiclassical initial value representation⁵⁻⁶ (LSC-IVR), also known as Wigner dynamics⁷⁻¹⁰), the forward-backward semiclassical dynamics (FBSD) method¹¹ and path integral Liouville dynamics¹² (PILD), use a quantized Boltzmann density in phase space to sample classical trajectories, accounting for zero-point energy and quantum dispersion. The use of classical trajectories for nonadiabatic dynamics (and more generally processes where a small system interacts with a large environment) is more challenging, because the formulations of classical and quantum mechanics are not readily compatible. A practical approach to nonadiabatic dynamics is offered by the mapping or MMST Hamiltonian¹³⁻¹⁴ and its coordinate-momentum phase space formulation that uses constrained variables.¹⁵⁻ ¹⁶ These approaches convert a discrete system to a continuous Hamiltonian that can be treated by classical trajectory-based methods, such as LSC-IVR and its more accurate symmetric quasiclassical windowing model. 17-18 Retaining the discrete nature of the system requires the interaction of local classical trajectories with delocalized wavefunctions. The most straightforward such scheme is the Ehrenfest method, ¹⁹ which is a mean field treatment that generally leads to poor results. ²⁰ Trajectory surface hopping ²¹⁻²² provides an ad hoc solution that addresses the most serious flaws of Ehrenfest's approach, but fails to properly account for decoherence from condensed phase environments.²³ A rigorous alternative is offered by the quantumclassical path integral²⁴⁻²⁵ (QCPI), in which classical trajectories interact consistently and unambiguously with quantum paths of the discrete system (which are also local), eliminating the need for mean field approximations or other assumptions. Another rigorous approach is based on the mixed quantum-classical Liouville equation²⁶⁻²⁷ (MQCL); however, its numerical implementation does not converge easily, thus MQCL is often used to obtain approximate results. Beyond classical trajectory-based methods, the centroid molecular dynamics²⁸⁻³⁰ (CMD) and ring-polymer molecular dynamics³¹⁻³³ (RPMD) approximations are widely used for simulating the dynamics in complex many-body systems. These methods extend the quantum-classical isomorphism³⁴ of the imaginary-time path integral formulation of quantum statistical mechanics³⁵ to extract dynamical information, and have been successfully applied to many processes.

Additional possibilities arise when the small system of interest interacts with a "bath" of harmonic degrees of freedom. The so-called system-bath Hamiltonian is widely employed as a simplified model for studying the dissipative effects of condensed phase environments on the dynamics of the observed system,³⁶ and also for simulating the effects of environments composed of normal mode vibrations, lattice phonons,

and even complex, unstructured environments such as liquids when the latter collectively induce Gaussian response.³⁷⁻³⁸ The path integral formulation of time-dependent quantum mechanics³⁹⁻⁴⁰ offers a unique advantage in this case, allowing harmonic bath degrees of freedom to be integrated out analytically.⁴¹ However, the resulting influence functional introduces memory effects that entangle the path integral variables, resulting in multidimensional integrals that cannot be sampled by Monte Carlo methods because the highly oscillatory nature of the quantum mechanical phase leads to a catastrophic sign problem, similar to (but arguably worse than) the situation encountered in equilibrium calculations with identical fermions.⁴²⁻⁴⁴

Numerically exact and stable methods for evaluating the real-time path integral were introduced in the 1990s with the development of the quasi-adiabatic propagator path integral⁴⁵⁻⁴⁹ (QuAPI). A number of further advances have led to methods that are highly efficient in particular regimes. In the special case of a bath characterized by the Debye spectral density, the path sum may be evaluated efficiently by solving hierarchical equations of motion⁵⁰⁻⁵¹ (HEOM). Further, the recent small matrix decomposition of the path integral⁵²⁻⁵⁴ (SMatPI) eliminates the demanding tensor storage requirements of the original QuAPI algorithm, allowing calculations in multistate systems and long memory. Recent SMatPI simulations of energy flow in the bacterial light harvesting complex, which treated explicitly the excited states of 24 bacteriochlorophyll molecules, each with 50 intramolecular vibrational modes,⁵⁵⁻⁵⁶ demonstrate the suitability of the algorithm for addressing highly nontrivial questions in biological and condensed phase processes. Since the SMatPI algorithm allows iterative propagation that involves the multiplication of small matrices (of minimal size, equal to that of the target reduced density matrix of the system), the main cost of the algorithm is the evaluation of the path sums over the entangled memory interval, which are utilized to construct the SMatPI matrices.

The purpose of the present paper is to introduce the kink sum, an efficient algorithm for evaluating the path sum in cases of strongly coupled baths that necessitate small time steps and induce long memory, thus leading to astronomical numbers of paths that make this regime inaccessible to available approaches. The key idea is the sparsity of path space in discrete systems, for which the weight of a path is closely related to the number and type of state-to-state transitions or kinks. Unlike earlier methods that utilized path selection based on the damping properties of the influence functional on forward-backward path pairs, the kink sum exploits the properties of the *system* propagator to systematically build the relatively small subset of contributing paths in forward time, which can be stored easily even when the memory is rather long and subsequently combined to generate only those forward-backward path pairs that contribute to the path sum. The kink sum algorithm is efficient and well-suited to strongly quantum mechanical regimes, where other path integral decompositions fail to converge, thus increasing the range of processes amenable to numerically exact treatment.

Section 2 presents an overview of the available path integral algorithms for system-bath Hamiltonians and describes the QuAPI representation of the reduced density matrix (RDM), along with its SMatPI decomposition. Section 3 shows that the set of paths consists of subsets with path weights that span many orders of magnitude, determined by the number and type of off-site steps a path takes. In the case of diagonal elements of the RDM for a two-level system (TLS), such steps form kinks, and these structures suggest the name of the algorithm. Section 4 shows that the kink sum can be performed analytically for a symmetric TLS, allowing one to easily assess the contribution from all paths in a subset containing a fixed number of kinks. Section 5 discusses how the selected subsets of paths can be most economically combined to form path pairs and to include the influence functional.

Section 6 illustrates the kink sum with results on four model systems that are representative of diverse physical situations: a symmetric TLS coupled to a bath with a very large reorganization energy, characteristic of self-exchange electron transfer reactions; a strongly asymmetric TLS typical of proton or energy transfer processes; the famous localization transition of a symmetric TLS at zero temperature; and a three-dimer system whose time evolution exhibits multiple time scales. In all these cases the kink sum converges easily, in spite of the very long memory. Last, a summary and some concluding remarks are given in section 7.

2. Small matrix path integral (SMatPI) and path summing algorithms

In the conventional case where the system sites are coupled to a common harmonic bath, the system-bath Hamiltonian is given by

$$\hat{H} = \hat{H}_0 + \sum_{i} \frac{\hat{p}_i^2}{2m} + \frac{1}{2} m \omega_i^2 \left(\hat{q}_i - \frac{c_i \hat{s}}{m \omega_i^2} \right)^2$$
 (2.1)

where

$$\hat{H}_0 = \sum_{i=1}^n \sum_{j=1}^n H_{ij} \left| \varphi_i \right\rangle \left\langle \varphi_j \right| \tag{2.2}$$

is the system Hamiltonian in the discrete (or DVR-discretized⁴⁶) basis φ_i , i = 1,...,n in which the position operator is diagonal, i.e.,

$$\hat{s} = \sum_{j=1}^{n} \sigma_{j} \left| \varphi_{j} \right\rangle \left\langle \varphi_{j} \right|, \tag{2.3}$$

and q_i , p_i are the harmonic bath coordinates and momenta. A somewhat different situation is frequently encountered in excitation energy transfer within molecular aggregates⁵⁷⁻⁵⁹ composed of many interacting units, where the electronic states of each unit are coupled to local harmonic baths consisting of intramolecular vibrational degrees of freedom. In such situations the total Hamiltonian can be expressed in system-bath form through a vector generalization⁶⁰ of Eq. (2.1) and (2.3),

$$\hat{H} = \hat{H}_0 + \sum_i \frac{\left|\hat{\mathbf{p}}_i\right|^2}{2m} + \frac{1}{2}m\omega_i^2 \left|\hat{\mathbf{q}}_i - \frac{\mathbf{c}_i \cdot \hat{\mathbf{s}}}{m\omega_i^2}\right|^2, \qquad \hat{\mathbf{s}} = \sum_{j=1}^n \boldsymbol{\sigma}_j \left|\varphi_j\right\rangle \left\langle \varphi_j\right|. \tag{2.4}$$

The vector system-bath Hamiltonian can be extended to include local, common and correlated baths, and leads to a particularly simple expression for the influence functional.⁶⁰ In order to keep the notation as simple as possible, the path integral variables are written in scalar form throughout the rest of this paper.

The RDM of the system is obtained by tracing the density matrix with respect to all bath degrees of freedom. At the time $N\Delta t$, the elements of the RDM for the initial condition $\left|s_0^+\right\rangle\left\langle s_0^-\right|$ are

$$\tilde{\rho}_{s_{x}^{+}s_{0}^{+}}^{(N0)} = \text{Tr}_{\text{env}} \left\langle s_{N}^{+} \middle| e^{-i\hat{H}t/\hbar} \middle| s_{0}^{+} \right\rangle \hat{\rho}_{b}(0) \left\langle s_{0}^{-} \middle| e^{i\hat{H}t/\hbar} \middle| s_{N}^{-} \right\rangle. \tag{2.5}$$

where $\hat{\rho}_b(0)$ is the initial density operator describing the bath, and the superscript (N0) indicates the final and initial times (in units of the path integral time step). It is useful to consider the full $n^2 \times n^2$ RDM that corresponds to all possible initial conditions. For brevity, this matrix is referred to as the RDM throughout this paper. In the discretized path integral formulation, the RDM elements are given by sums of amplitudes,

$$\tilde{\rho}_{s_{N}^{\pm}s_{0}^{\pm}}^{(N0)} = \sum_{s_{N-1}^{\pm}=\sigma_{1}}^{\sigma_{n}} \cdots \sum_{s_{1}^{\pm}=\sigma_{1}}^{\sigma_{n}} K_{s_{N}^{+}, s_{N-1}^{+}} \cdots K_{s_{1}^{+}, s_{0}^{+}} K_{s_{N}^{-}, s_{N-1}^{-}} \cdots K_{s_{1}^{-}, s_{0}^{-}} F_{s_{N}^{\pm}, s_{N-1}^{\pm}, \dots, s_{0}^{\pm}},$$

$$(2.6)$$

along all discrete forward-backward paths $s_N^\pm \cdots s_0^\pm$ associated with the time points that separate short-time propagators. Here $K_{s_k^+s_{k-1}^+}$ are the forward-backward system propagators and $F_{s_k^\pm s_k^\pm}^{kk'}$ are the QuAPI-discretized influence functional factors.⁴⁹

The path integral variables in Eq. (2.6) are fully entangled within the memory length induced by the bath. The SMatPI decomposition⁵²⁻⁵³ disentangles the path integral variables by recursively shifting the entanglement to longer time intervals. Specifically, the path sum for each auxiliary RDM matrix $\mathbf{R}^{(r_0)}$, r = 2,3,... (with continuation, i.e. non-endpoint influence functional coefficients⁵³) is expressed as a sum of matrix products that involve earlier auxiliary RDMs, as well as an entangled residual $\mathbf{M}^{(r_0)}$,

$$\mathbf{R}^{(20)} = \mathbf{M}^{(21)} \cdot \mathbf{R}^{(10)} + \mathbf{M}^{(20)},$$

$$\mathbf{R}^{(30)} = \mathbf{M}^{(32)} \cdot \mathbf{R}^{(20)} + \mathbf{M}^{(31)} \cdot \mathbf{R}^{(10)} + \mathbf{M}^{(30)},$$
(2.7)

etc. It has been shown analytically⁵²⁻⁵³ that the residual decreases rapidly once the memory length has been exceeded and thus can be dropped after some entanglement length r_{max} , which in practice is equal to (but may also be smaller than⁵⁴) the memory length induced by the bath. Discarding the negligible residual $\mathbf{M}^{(r_{\text{max}}+1,0)}$ leads to the following expression of the auxiliary RDM at times longer than the entanglement length:

$$\mathbf{R}^{(N0)} = \sum_{r=1}^{r_{\text{max}}} \mathbf{M}^{(N,N-r)} \cdot \mathbf{R}^{(N-r,0)}, \quad N = r_{\text{max}} + 1, \dots$$
 (2.8)

By construction, Eq. (2.8) is an exact decomposition of the path integral. The $n^2 \times n^2$ SMatPI matrices $\mathbf{M}^{(N,N-r)}$ are given by the residuals (with proper influence functional coefficients suitable for continuation⁵³) and involve fully entangled path sums within the entangled memory interval. With proper influence functional boundary conditions, these auxiliary matrices give the desired full RDM $\tilde{\boldsymbol{\rho}}^{(N0)}$.

To compute the SMatPI matrices, one must be able to evaluate the path sum within the entanglement length by one of several available methods. The largest such calculation involves n^4 sums, each of which contains $n^{2(r_{\text{max}}-1)}$ terms:

$$R_{s_{r_{\max}}^{+}s_{0}^{\pm}}^{(r_{\max}0)} = \sum_{s_{r_{\max}-1}^{\pm}=\sigma_{1}}^{\sigma_{n}} \cdots \sum_{s_{1}^{\pm}=\sigma_{1}}^{\sigma_{n}} K_{s_{r_{\max}}^{+}s_{r_{\max}}^{+}} \cdots K_{s_{1}^{+}s_{0}^{+}} K_{s_{N}^{-}s_{N-1}} \cdots K_{s_{1}^{-}s_{0}^{-}} F_{s_{r_{\max}}^{\pm}s_{r_{\max}-1}^{\pm}\dots s_{0}^{\pm}}.$$

$$(2.9)$$

The simplest and most direct approach for evaluating Eq. (2.9) is to explicitly construct all forwardbackward path sequences $s_{r_{\text{max}}}^{\pm}, s_{r_{\text{max}}-1}^{\pm}, \dots, s_{0}^{\pm}$. This is a straightforward task if the number of system states and the entanglement parameter are reasonably small. For example, for n = 2 the direct evaluation of the path sum is extremely fast for $r_{\text{max}} \leq 10$ and can be obtained with modest effort for entanglement lengths up to approximately $r_{\text{max}} \simeq 20$. Large values of r_{max} are accessible by applying filtering techniques, which exploit the damping role of the influence functional, implying that the vast majority of the paths leads to exponentially small contributions. Early work⁶¹⁻⁶² used Monte Carlo methods to obtain the statistically significant path sequences (those with a weight larger than a specified threshold) for use in iterative QuAPI calculations. Subsequent work⁶³⁻⁶⁴ developed deterministic procedures for constructing the set of contributing paths. Such procedures, which build the paths step-by-step, are free of Monte Carlo error but require the storage of all retained forward-backward sequences, which often is impractical. The simplest storage-free approach is to generate all sequences in a loop, immediately discarding forward-backward path combinations if the product of system propagators (along with the single-step influence functional factors) falls below the threshold, proceeding to evaluate the influence functional only for those that satisfy the weight criteria. 65-66 This procedure avoids the majority of effort for path sequences that make negligible contributions, but the mere step of generating them restricts in practice the range of accessible r_{max} values.

It is formally possible to reduce the number of terms in the forward-backward path sum by switching to the blip representation.⁶⁷ This involves performing a change of variables at each time point from s_k^+, s_k^- to the "blip" and "sojourn" variables $\Delta s_k = s_k^+ - s_k^-$, $\overline{s}_k = \frac{1}{2} \left(s_k^+ + s_k^- \right)$. By exploiting the structure of the influence functional, all sojourn variables are summed using efficient matrix multiplication, effectively reducing the number of terms to $\left(\frac{1}{2} n(n+1) \right)^{r_{\text{max}}-1}$, a number much smaller than the number $n^{2(r_{\text{max}}-1)}$ of terms in the original coordinates. Thus, the *blip transformation* leads to an exponential acceleration of the path sum. For example, with n=2 the total number of terms becomes $3^{r_{\text{max}}-1}$, which for $r_{\text{max}} >> 1$ is a much smaller number than $4^{r_{\text{max}}-1}$, pushing the practical limit from $r_{\text{max}} \simeq 20$ to $r_{\text{max}} \simeq 25$.

In cases of near-classical, strongly dissipative environments (large system-bath coupling, low-frequency modes, moderate-to-high temperature), the *blip decomposition* exploits the exponential decrease in the path weight with increasing number of blips, leading to an exponential reduction of the number of terms. Only the surviving forward-backward blip configurations (rather than the full path sequences) need to be generated, accounting for all spin-sojourn influence functional interactions between blips through iterative matrix multiplication.⁶⁷ Since the required number of blips tends to be small in strongly dissipative regimes, the blip decomposition can converge rapidly even with $r_{max} > 100$ in such situations.

Another option suitable for strongly coupled, low-frequency baths is offered by the quantum-classical path integral²⁴⁻²⁵ (QCPI), a rigorous quantum-classical methodology applicable to complex anharmonic environments. QCPI captures the effects of the bath through classical trajectories that interact locally with system paths, and offers an exact, fully quantum mechanical approach to system-bath Hamiltonians. It has been shown that the dissipative effects associated with classical decoherence processes⁶⁸ can be fully included in appropriately augmented system propagators,⁶⁹ such that the remaining path sum must account only for the quantum mechanical component of the bath-induced memory, and even the latter can be partially incorporated through a dynamically consistent scheme.⁷⁰ As a result, the QCPI time step can be considerably larger and convergence is achieved with shorter memory. Recent work⁷¹ showed that in spite of small Monte Carlo errors, QCPI may be employed for efficient calculation of SMatPI matrices.

A different approach⁷² takes advantage of the structure of the influence functional to express the forward-backward path amplitude in the form of a matrix product state⁷³ (MPS). Formally, the size ("bond dimension") of the resulting matrices increases exponentially with r_{max} , following the number of paths, but is kept much smaller by utilizing singular value decomposition (SVD) to compress the matrices. A high level of compression is feasible under weak system-bath coupling, reflecting the enormous redundancy of the QuAPI tensor and making the time-evolving matrix product operator (TEMPO) method⁷² an excellent approach for constructing the SMatPI matrices in small systems with favorable parameters.⁶⁶ However, strong coupling and multi-state systems quickly lead to large bond dimensions, and since SVD scales as the third power of matrix size, the computational cost (storage and number of operations) of TEMPO becomes prohibitive in such situations.

3. Paths and kinks

To address these challenges, the present paper introduces a systematic and efficient procedure for dramatically reducing the number of paths employed in the calculation of the RDM, thus allowing evaluation of the path sum over long entanglement intervals in regimes that are unfavorable to the approaches discussed in the previous section. Unlike earlier methods that were based on the weights of forward-backward path pairs, the present approach focuses on the much smaller set of paths along the *forward* time direction. Path weights are therefore based on properties of the system Hamiltonian alone, although additional benefits deriving from the influence functional contribute to the efficiency of the method at a later stage.

Consider the set of discrete *forward* paths over a length of r time steps, where the largest value of r is the entanglement length (or, if the dynamical process is short-lived, the entire propagation length). The wavefunction that evolves from the state $\left|s_{0}^{+}\right\rangle$ (i.e. the propagator) of the isolated system is given by the (single) path sum

$$\Psi_{s_r,s_0}^{(r0)} = \sum_{s_{r-1}=\sigma_1}^{\sigma_n} \cdots \sum_{s_1=\sigma_1}^{\sigma_n} K_{s_r,s_{r-1}} \cdots K_{s_1,s_0} . \tag{3.1}$$

Eq. (3.1) is the forward-time analogue of the RDM in Eq. (2.5). To compute the value of $\Psi_{s_r,s_0}^{(r0)}$, one needs to add the amplitudes of the n^{r-1} paths that span the time points 0,...,r. The amplitude of a path is determined by the number of short-time propagator factors K_{11} , the number of K_{12} factors, the number of K_{13} factors, etc. In general, there are n(n+1)/2 distinct propagator elements, although symmetry may reduce this number. (For example, in a symmetric TLS there are only two propagator elements, because $K_{11} = K_{22}$.) The number m(n,r) of possible values for the total path amplitude is equal to the number of connected graphs with n vertices (see Figure 1). In general, this number grows rapidly with n and/or r. Thus, the set of paths is divided into m(n,r) equivalence classes, each of which consists of all paths that have the same amplitude. It follows that the paths within each equivalence class interfere constructively, while paths that belong to different equivalence classes may interfere constructively or destructively.

Suppose all short-time propagator elements have different values and (without loss of generality) that K_{11} has the largest modulus. The path with the largest weight, equal to $(K_{11})^r$, is the one that has all coordinates equal to σ_1 , and the corresponding equivalence class contains a single element. On the other

hand, if all diagonal propagator elements have the same value (as in a cyclic system with identical site energies), then the equivalence class of largest weight includes n paths. The next equivalence class is obtained by replacing a single K_{11} factor by the short-time propagator of next-to-largest magnitude (preserving the connected topology that characterizes a path). If this propagator element can be inserted at any of the r time intervals, it generates an equivalence class with r paths. Inserting multiple short-time propagators of smaller magnitudes leads to large numbers of paths with rapidly decreasing weights. As r increases, so does the number of equivalence classes, some of which contain huge numbers of paths, each of a very small weight. Whether or not such subsets contribute substantially to the desired path sum depends on the balance between a path's weight and the cardinality of the subset. As one sums the paths grouped into equivalence classes with decreasing path weights, the contributions go through a maximum and subsequently decay rapidly.

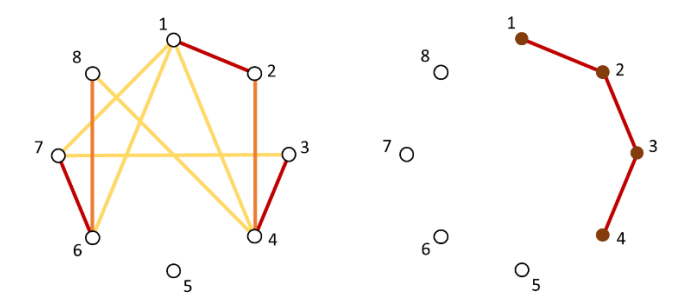


Fig. 1. Graphs showing two 10-step paths that start and ends on site 1 in a system of 8 sites, represented by hollow black circles. Filled circles and lines indicate elementary path segments. Burgundy circles indicate diagonal short-time propagator elements, while red, orange and yellow lines correspond to propagator elements connecting nearest-, next-nearest-neighbor and distant sites, respectively. The left graph shows a path consisting of the sequence 1-2-4-3-7-6-1-4-8-6-1, while the right graph shows the path 1-1-2-3-3-3-4-3-2-1-1.

For small time steps, off-diagonal elements of the propagator for discrete Hamiltonians have much smaller values than diagonal elements, regardless of the site energy values. Off-diagonal elements may also vary significantly in value, depending primarily on the coupling elements in the system Hamiltonian. These facts imply that the contribution of a path to the wavefunction value is governed by the number and type of off-diagonal propagator factors, which correspond to transitions between states. In the case of a symmetric TLS with $s_r = s_0$, paths hop between the two states an even number of times, forming an integer number of (tight or loose) kinks, where each kink includes two off-diagonal short-time propagator elements (see Figure 2 in the next section). In multistate systems, kinks are segments where a path departs from a state φ_i at a particular instant, travels to another state or to several other states, and eventually returns to φ_i after two or more time steps. Paths containing multiple kinks make exponentially small contributions to the path sum for the wavefunction, Eq. (3.1). To calculate the value of the wavefunction at $r\Delta t$, one must sum the amplitudes of all paths that contribute to the desired accuracy. This task can be achieved by sorting the paths according to the number/type of kinks they contain. In multistate systems it is not necessary to bin the paths into all possible equivalence classes, although doing so offers some benefits.⁷⁴ Instead, one may group together paths of similar weights, generating a small number of bins that store the coordinates of the contained paths.

Before proceeding to make these ideas suitable for evaluation of the RDM that contains influence functional factors, it is instructive to discuss the simplest and most common example, a symmetric TLS.

4. Analytical example: symmetric two-level system

As an example, consider a symmetric TLS described by the Hamiltonian

$$\hat{H}_0 = -\hbar\Omega(|\varphi_1\rangle\langle\varphi_2| + |\varphi_2\rangle\langle\varphi_1|) \tag{4.1}$$

The focus is on evaluation of the wavefunction at the time $r\Delta t$ with initial and final conditions set at the first site, $\Psi_{11}^{(r0)} = \langle \varphi_1 | e^{-iH_0r\Delta t/\hbar} | \varphi_1 \rangle$. Since the two site energies are identical in the case of a symmetric TLS, there are only two independent propagator elements, with values

$$K_{11} = K_{22} = \cos \Omega \Delta t, \quad K_{12} = i \sin \Omega \Delta t$$
 (4.2)

In this case each kink contains two K_{12} factors. Fig. 2 shows various arrangements of paths with zero, one and two kinks.

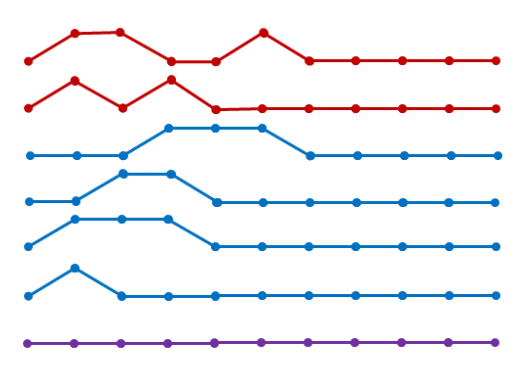


Fig. 2. Some representative discretized paths for a TLS over N = 10 time steps. Violet: path with no kinks. Blue: representative paths with one kink. Red: representative paths with two kinks.

There is a single kink-free path whose contribution is equal to $(K_{11})^r$. The number of paths with one kink is given by the number of possible arrangements of two K_{12} elements over r time steps, i.e. is equal to

$$\binom{r}{2} = \frac{r!}{2!(r-2)!} \,. \tag{4.3}$$

Each such path has an amplitude equal to $K_{11}^{r-2}K_{12}^2$. Similarly, the number of paths with amplitude equal to $K_{11}^{r-4}K_{12}^4$ is given by the number of arrangements of four off-diagonal propagator elements over r steps,

etc. Figure 4 shows the number of paths with a particular number of off-diagonal propagator elements as a function of path length. Table 1 shows the equivalence classes, their cardinalities, the amplitude of a path in each equivalence class, and the total contribution of an equivalence class, for an even value of r.

The sum of amplitudes along all paths is thus given by

$$\Psi_{11}^{(r0)} = (\cos \Omega \Delta t)^{r} + \frac{r!}{2!(r-2)!} (\cos \Omega \Delta t)^{r-2} (i \sin \Omega \Delta t)^{2} + \frac{r!}{4!(r-4)!} (\cos \Omega \Delta t)^{r-4} (i \sin \Omega \Delta t)^{4} + \dots + (i \sin \Omega \Delta t)^{r}$$
(4.4)

It is easy to see that the terms in Eq. (4.4) are the even powers in the Taylor expansion of the binomial $(\cos \Omega \Delta t + i \sin \Omega \Delta t)^r$, and therefore the sum is equal to

$$\Psi_{11}^{(r0)} = \frac{1}{2} \left[\left(\cos \Omega \Delta t + i \sin \Omega \Delta t \right)^r + \left(\cos \Omega \Delta t - i \sin \Omega \Delta t \right)^r \right] = \cos r \Omega \Delta t \tag{4.5}$$

which is recognized as the exact result for the diagonal element of the system propagator at the time $r\Delta t$.

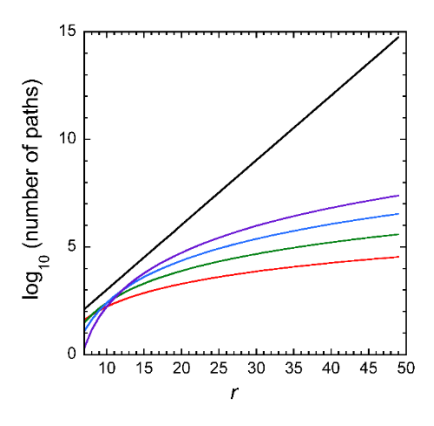


Fig. 3. Number of discrete paths with 3-6 off-diagonal elements as a function of the number *r* of time steps. Red, green, blue and violet show the number of paths with 3,4,5 and 6 off-diagonal factors. The solid black line shows the number of all possible paths.

Table 1.

equivalence class	number of K_{11} factors	number of K_{12} factors	path amplitude	cardinality	total contribution
1	r	0	$(\cos \Omega \Delta t)^r$	1	$(\cos \Omega \Delta t)^r$
2	r-2	2	$(\cos\Omega\Delta t)^{r-2}(i\sin\Omega\Delta t)^2$	$\frac{r!}{2!(r-2)!}$	$-\frac{r!}{2!(r-2)!}\cos^{r-2}\Omega\Delta t\sin^2\Omega\Delta t$
3	r-4	4	$(\cos\Omega\Delta t)^{r-4}(i\sin\Omega\Delta t)^4$	$\frac{r!}{4!(r-4)!}$	$\frac{r!}{4!(r-4)!}\cos^{r-4}\Omega\Delta t\sin^4\Omega\Delta t$
$\frac{1}{2}r + 1$	0	r	$(i\sin\Omega\Delta t)^r$	1	$(-1)^{\frac{r}{2}}\sin^r\Omega\Delta t$

Since $|\sin\Omega\Delta t|\ll|\cos\Omega\Delta t|$ as $\Delta t\to 0$, the contribution of a path to the total amplitude decreases monotonically and rapidly as the number of kinks increases. However, the binomial coefficient that gives the number of paths with κ kinks also increases rapidly with κ at first, reaching its maximum at $\kappa=\frac{1}{2}r$, and subsequently decreases again in a symmetric fashion. Figure 4 (left panel) shows the absolute value of the path amplitude and number of paths as a function of the number of kinks at the time $t=5\Omega^{-1}$ with r=100 (such that $\Delta t=0.05\Omega^{-1}$). The total contribution of all paths with the same number of kinks is shown in the right panel of Figure 4. Table 2 shows the corresponding numerical values for paths with contribution greater than 10^{-4} . The simplest path that remains on state φ_1 at all times contributes to the amplitude a value slightly smaller than unity. One-kink paths add to a large negative contribution. Two-kink paths have very small individual amplitudes ($\sim 10^{-6}$) but the total contribution of nearly four million such paths exceeds unity. As the number of kinks is increased, individual path amplitudes drop off rapidly, but their number increases, leading to significant contributions to the wavefunction up to $\kappa = 8$. With $\kappa \geq 9$ kinks the path amplitude is so small that the large number of such paths no longer compensates, making collective contributions that are corrections smaller than 10^{-4} . If one is interested in computing the total amplitude through four decimal places, including paths with ten or more kinks is entirely unnecessary.

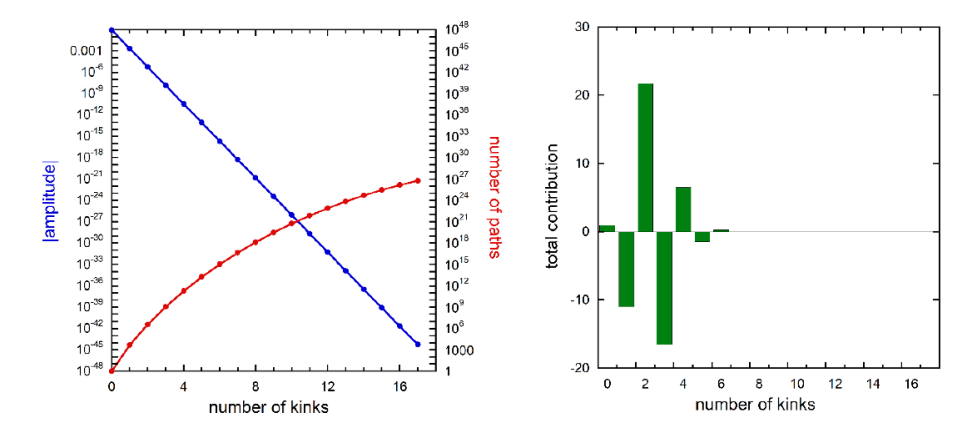


Fig. 4. Left: Path amplitude (blue) and subset cardinality (red) as a function of the number of kinks with the parameters given in the text. Right: Total contribution from all paths with the same number of kinks. Note the large contributions of each group of paths in relation to the net sum, i.e. the wavefunction value, 0.28366.

Table 2. Path amplitude, number of paths and overall contribution to the probability of remaining in the state φ_1 as a function of the number of kinks for $t = 5\Omega^{-1}$ with r = 100, $\Delta t = 0.05\Omega^{-1}$.

# of kinks	path amplitude	# of paths	contribution
0	+0.882451	1	+0.88245
1	-2.2098E-03	4,950	-10.93856
2	+5.5337E-06	3,921,225	+21.69906
3	-1.3857E-08	1.1921E09	-16.51881
4	+3.4701E-11	1.8609E11	+6.45752
5	-8.6898E-14	1.7310E13	-1.50424
6	+2.1761E-16	1.0504E15	+0.22858
7	-5.4493E-19	4.4187E16	-0.02408
8	+1.3646E-21	1.3459E18	+0.00184
9	-3.4172E-24	3.0665E19	-0.00010

With the chosen parameters, the largest contribution comes from two-kink paths. If r were to be increased for a fixed total time, the contributions of paths with more kinks would increase. If the time step is decreased for a fixed value of r, the weights of paths with a given number of kinks decreases, leading to faster convergence of the series, but the total propagation time reached is shorter.

Summing all the contributions with up to $\kappa = 9$ gives the approximate wavefunction value 0.28366. This value is in excellent agreement with the exact result $\Psi_{11}^{(50)} = \cos 5$.

5. Forward-backward paths and influence functional

Propagation of a system's wavefunction involves the set of Q paths whose weights are larger than a chosen threshold. The RDM includes forward-backward path pair combinations with amplitudes that are augmented by influence functional factors. While the array of Q paths is usually manageable, the set of contributing forward-backward paths often exceeds realistically available computer storage. Rather than constructing and storing forward-backward path pairs, the kink algorithm combines the set of forward paths with the (same) set of backward paths. However, the number Q^2 of forward-backward paths that enter the double sum may be prohibitively large. Fortunately, for reasons that are discussed below, the forward-backward path sum usually converges with a much smaller number of terms.

First, amplitudes multiply in the forward-backward pair. As a result, combining a forward path of the smallest retained weight with a backward path of comparable amplitude will lead to a contribution that is by far smaller than the desired accuracy in the RDM. Phrased differently, the $Q \times Q$ matrix of forward-backward paths is fairly sparse. The arrangement of paths into equivalence classes, or in merged such subsets that form bins, allows the treatment of only those forward-backward combinations expected to make an appreciable contribution to the sum, avoiding a double loop over all Q^2 terms. Convergence is easily checked by increasing the number of forward-backward bin combinations.

Second, the influence functional decreases the weights of forward-backward path combinations to values far below those of the bare system. Consider the paths over a large number of time steps with a small number of kinks. In the vast majority of forward-backward path combinations, the kinks of the forward and backward paths will not align, leading to multiple blip intervals that lead to an exponential decrease of the pair's weight. This damping implies that bins whose overall contribution may be important in the absence of a bath can amount to negligible corrections once the influence functional is included, effectively increasing the path selection threshold and decreasing the number Q of retained sequences. For example, the analysis presented in the previous subsection suggests that paths with up to nine kinks must be included for the given parameters, but when computing the RDM in the presence of system-bath coupling one may find that bins with up to four or five kinks are sufficient.

6. Illustrative examples

This section illustrates the use of the kink sum algorithm in the evaluation of the SMatPI matrices with several examples. In all cases the system states are coupled to common or local baths described by an Ohmic spectral density,

$$J(\omega) = \frac{1}{2} \pi \xi \omega e^{-\omega/\omega_{c}} \tag{6.1}$$

where ξ indicates the system-bath coupling strength and $\omega_{\rm c}$ is a cutoff frequency.

(i) Symmetric (self-exchange) electron transfer model

Simulating the dynamics of charge transfer processes often provides a serious challenge. This is so because such processes are frequently characterized by a large reorganization energy, which necessitates a small time step and gives rise to long memory. The surrounding medium may contain strongly coupled high-frequency modes, which are primarily in their ground state even at ambient temperatures, generating significant quantum effects. Because of the long quantum memory, the blip series does not converge rapidly under such conditions. This regime has generally been inaccessible to numerically exact methods.

Figure 5 shows results for a model symmetric electron transfer pair, described by the system Hamiltonian

$$\hat{H}_0 = -\hbar\Omega(|\varphi_1\rangle\langle\varphi_2| + |\varphi_2\rangle\langle\varphi_1|) \tag{6.2}$$

whose states are coupled to a common Ohmic bath representative of a molecular solvent or biological medium through the position operator given by Eq. (2.3) with $\sigma_1 = 0$, $\sigma_2 = 2$ at an inverse temperature $\hbar\Omega\beta = 0.5$. The bath parameters are $\xi = 2$, $\omega_c = 20\Omega$, such that the strongest coupled modes are in their respective ground states ($\hbar\omega_c\beta = 10$). The bath is initially in equilibrium with the donor (state φ_1). The solvent reorganization $\lambda = 80\hbar\Omega$ is very large, such that a very small time step $\Omega\Delta t = 0.01$ is required for convergence of the path integral. Accurate results with the kink sum algorithm were easily obtained for entanglement lengths up to $r_{max} = 70$, which is adequate for convergence, using paths containing up to 5 off-diagonal short-time propagator elements over the time points 1,...,r-1. The path sum was restricted to forward-backward combinations containing at most seven K_{12} factors. The RDM was propagated for a total of N = 250000 steps, providing results up to $\Omega t = 2500$.

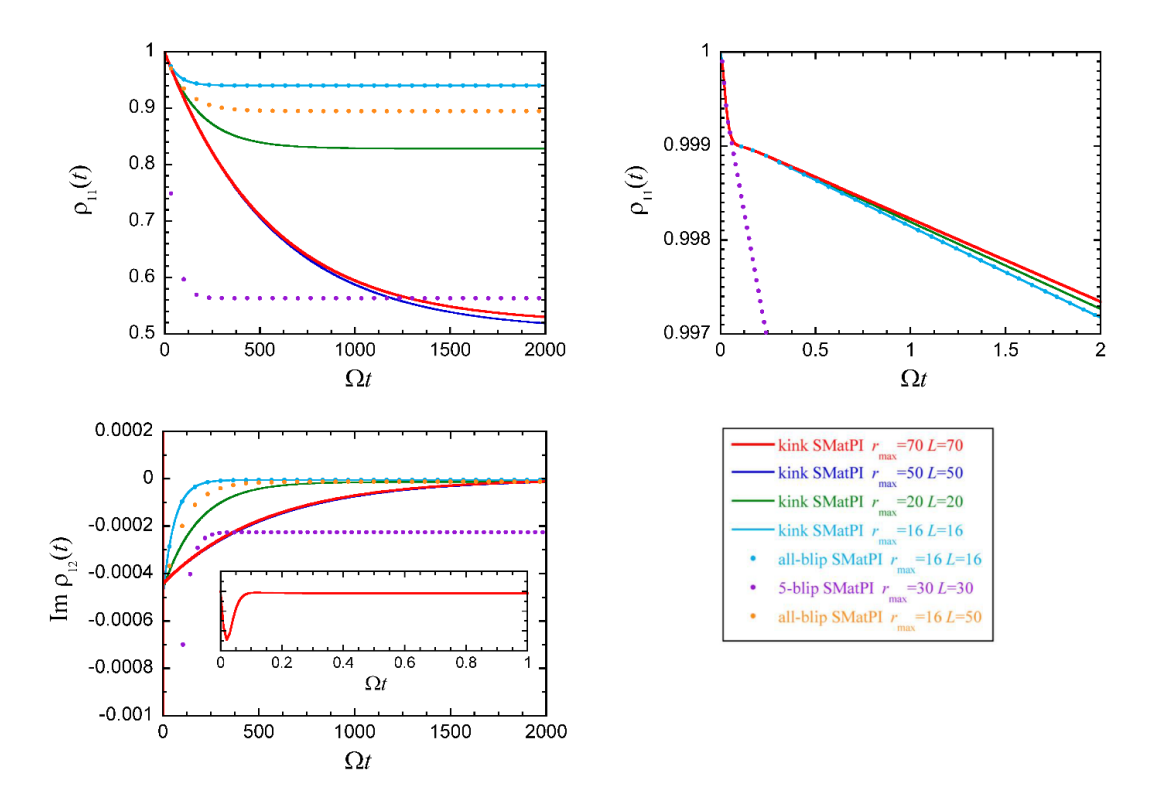


Fig. 5. RDM elements for a model charge transfer reaction. The donor-acceptor pair is coupled to an Ohmic bath with $\xi=2$, $\omega_{\rm c}=20\Omega$ at an inverse temperature $\hbar\Omega\beta=0.5$. Top left: donor population over 200000 path integral time steps. Kink-SMatPI results are shown for $r_{\rm max}=16,20,50$ and 70. The SMatPI matrices employed paths containing up to 5 off-diagonal propagator elements over the time points $1,...,r_{\rm max}-1$.

As seen in the top left panel of Fig. 5, if shorter memory is used to construct the SMatPI matrices, the donor population does not equilibrate properly, eventually reaching long-time populations that are much higher than 0.5. Similarly, longer-memory calculations with SMatPI matrices obtained using an inadequate number of blips cause the population to decay too rapidly. Note that differences among unconverged results (top right panel) are very small during early times and could easily be ignored, leading to a false perception of convergence. Also, a much faster decay is observed at very short times, before the population settles into exponential dynamics.

The bottom panel of Fig. 5 shows the imaginary part of the off-diagonal element of the RDM. Off-diagonal RDM elements arise from quantum superpositions, and their imaginary components are related to instantaneous population derivatives.⁷⁵ In the case of a TLS,⁷⁶ $\Omega \operatorname{Im} \tilde{\rho}_{12}(t)$ gives the time derivative of $\tilde{\rho}_{11}(t)$ and thus decays to zero on the same time scale as the donor population. As shown in the right bottom panel, this function displays a clear plateau characteristic of the reactive flux at short times, following some early highly nonmonotonic behavior.

(ii) Exothermic energy transfer model

The second example is representative of excitation energy transfer in a model heterodimer. The excited states of the monomers are coupled by the parameter $-\hbar\Omega$ and have energies that differ by the asymmetry parameter $\varepsilon=10\hbar\Omega$ according to the Frenkel exciton Hamiltonian^{58,77-79}

$$\hat{H}_{0} = \varepsilon \left| \varphi_{1} \right\rangle \left\langle \varphi_{1} \right| - \hbar \Omega \left(\left| \varphi_{1} \right\rangle \left\langle \varphi_{2} \right| + \left| \varphi_{2} \right\rangle \left\langle \varphi_{1} \right| \right). \tag{6.3}$$

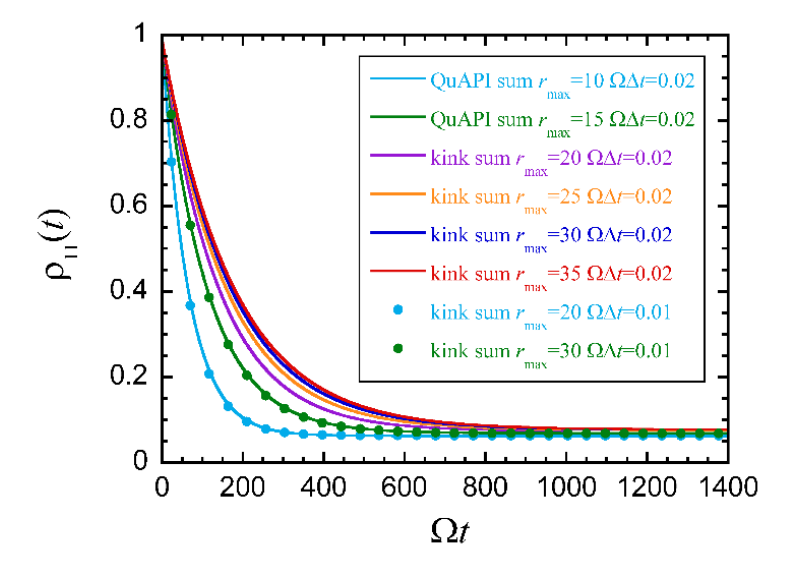


Fig. 6. Donor population in a strongly exothermic charge transfer reaction modeled by an asymmetric TLS coupled to an Ohmic bath with $\xi=2$, $\omega_{\rm c}=10\Omega$ at an inverse temperature $\hbar\Omega\beta=0.25$. The asymmetry parameter is $10\hbar\Omega$. The lines show SMatPI results with $\Omega\Delta t=0.02$ and $r_{\rm max}=10-35$. For $r_{\rm max}=10$ and 15 the SMatPI matrices were computed from the full QuAPI path sum, while the kink sum algorithm was used for $r_{\rm max}=20-35$. The markers show kink sum results with $\Omega\Delta t=0.01$, verifying convergence with respect to time step value.

Energy transfer follows excitation of the first monomer from the ground state via a Franck-Condon process. The two excited states are coupled to local baths with $\xi = 2$, $\omega_c = 10\Omega$ at an inverse temperature $\hbar\Omega\beta = 0.25$, such that both the system and the strongest coupled modes are at a moderately low temperature ($\beta\varepsilon = \hbar\omega_c\beta = 2.5$). The bath reorganization energy of each unit is $40\hbar\Omega$.

Figure 6 shows SMatPI results obtained using a path integral time step $\Omega \Delta t = 0.02$ over entanglement lengths ranging from $r_{\rm max} = 10$ to $r_{\rm max} = 35$. Convergence with respect to the time step was confirmed through calculations with $\Omega \Delta t = 0.01$. For $r_{\rm max} = 10-15$ the results computed with the kink sum algorithm are in agreement with those obtained with the full, unfiltered QuAPI path sum method. The donor population converges with $r_{\rm max} = 35$.

(iii) TLS localization

It is well-known⁸⁰ that a symmetric TLS coupled to a high-frequency ($\omega_c >> \Omega$) Ohmic bath at zero temperature undergoes a transition to a localized phase when the coupling to the bath exceeds the critical value $\xi=1$. The TLS Hamiltonian is given by Eq. (6.2) and the system operator has $\sigma_1=1,\sigma_2=-1$. The TLS states are coupled to a common Ohmic bath with parameters $\omega_c=10\Omega$, $\xi=1.5$. At zero temperature, these parameters represent a highly quantum mechanical regime.

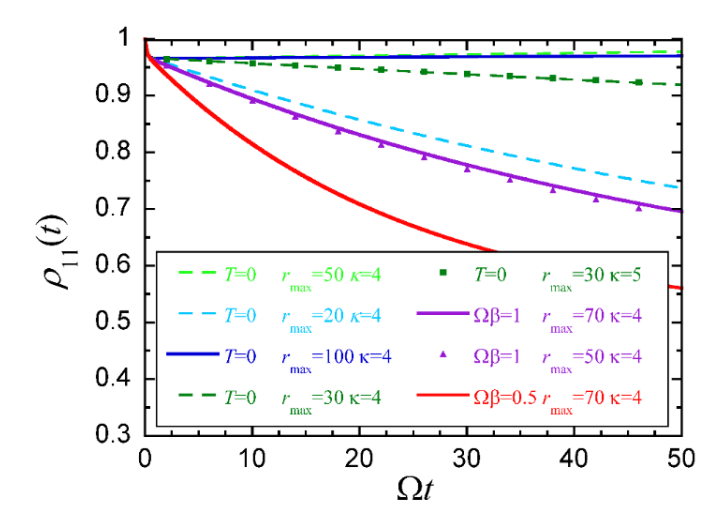


Fig. 7. Localization transition as a function of temperature in a symmetric TLS strongly coupled to an Ohmic bath. The SMatPI results were obtained with $\Omega \Delta t = 0.02$ and $r_{max} = 20 - 100$ with matrices computed with the kink sum algorithm with up to 5 off-diagonal propagator elements. Results are shown at zero temperature and also for $\hbar\Omega\beta = 1$ and 0.5.

Figure 7 shows the time evolution of the initially populated state with the bath in its ground state and also at two temperatures specified by $\hbar\Omega\beta=1$ and $\hbar\Omega\beta=0.5$. The SMatPI matrices were computed using the kink sum algorithm with entanglement lengths up to $r_{\rm max}=100$, using a path integral time step $\Omega\Delta t=0.02$. The calculations employed the kink sum algorithm with 4-5 off-diagonal propagator elements, which result in a very small number of paths in comparison with the total number of $2^{200} \approx 1.6 \times 10^{60}$ paths that enter the sum for the RDM. At zero temperature the converged population remains constant after a minor short-time drop, in excellent agreement with analytical treatments⁸⁰ and earlier path integral calculations. However, finite temperature is seen to rapidly destroy localization, causing the population to decay, even though the bath modes that are most strongly coupled to the TLS are still at a very low temperature ($\hbar\omega_c\beta=10$ and 5, respectively).

(iv) Transport in a three-dimer model with multiple time scales

Last, the kink sum algorithm is applied to a model of transport in a cluster of three molecular dimers in a linear arrangement (see Figure 8), with a total of six electronic states. The system Hamiltonian is given by

$$\hat{H}_{0} = -\hbar\Omega(|\varphi_{1}\rangle\langle\varphi_{2}| + |\varphi_{3}\rangle\langle\varphi_{4}| + |\varphi_{5}\rangle\langle\varphi_{6}|) - J(|\varphi_{2}\rangle\langle\varphi_{3}| + |\varphi_{4}\rangle\langle\varphi_{5}|) + \text{h.c.}$$
(6.4)

where $-\hbar\Omega$ is the intra-dimer electronic coupling, -J is the inter-dimer coupling, and h.c. denotes the hermitian conjugate. The inter-dimer coupling parameter is chosen as $J=0.1\hbar\Omega$. The electronic state of each monomer is strongly coupled to its own vibrational bath modeled by an Ohmic spectral density with parameters $\xi=2$, $\omega_{\rm c}=10\Omega$ at a temperature $\hbar\Omega\beta=0.25$, which is intermediate for the bath ($\hbar\omega_{\rm c}\beta=2.5$). Only state φ_3 is initially populated. The three characteristic frequencies $\omega_{\rm c}=10\Omega=100J/\hbar$, which span

two orders of magnitude, give rise to multiple time scales that are observed in the RDM evolution and which necessitate long-time propagation with a small time step.

SMatPI results are shown in Figures 8 and 9 over N = 500000 path integral time steps of length $\Omega \Delta t = 0.02$. Convergence was obtained with entanglement length $r_{\text{max}} = 25$. The SMatPI matrices were efficiently computed with the kink sum algorithm. The full set of forward-backward paths with these parameters involves $6^{50} = 8 \times 10^{38}$ terms.

The three characteristic frequencies, each separated from the next by an order of magnitude, are readily identified in the population dynamics shown in Fig. 8. The initially populated state is seen to decay to approximately 0.5 within a time $\Omega t \simeq 1000$, transferring its population to state φ_4 within the same central dimer. During this early time period the populations of the edge dimers begin to grow, with $\tilde{\rho}_{22}$ rising first because it is coupled to the initially populated state φ_3 , while $\tilde{\rho}_{55}$ follows with a delay because it receives population from state φ_4 , and the most distant $\tilde{\rho}_{66}$ begins to grow even slower. Once the central dimer has reached internal equilibrium, a much slower exponential decay of $\tilde{\rho}_{33}$ and $\tilde{\rho}_{44}$ is observed, which is accompanied by population transfer to the edge dimers.

Fig. 9 shows the imaginary components of some off-diagonal RDM elements. While the most informative and intuitive picture is obtained from the evolution of coherence maps, 81 the present focus is on the effect of multiple time scales on the rates of intra- and inter-dimer transfer. Recent work showed 75 that imaginary RDM elements are related to instantaneous time derivatives of state populations. For the present system,

$$\frac{d}{dt}\tilde{\rho}_{33}(t) = 2\Omega \operatorname{Im}\tilde{\rho}_{34}(t) + \frac{2J}{\hbar} \operatorname{Im}\tilde{\rho}_{32}(t)$$
(6.5)

As seen in Fig. 9, $\operatorname{Im} \tilde{\rho}_{34}(t)$ and $\operatorname{Im} \tilde{\rho}_{32}(t)$ (and also the linear combination in Eq. (6.5)) display characteristic plateaus early on, which are associated with the rapid intra-dimer dynamics. However, once the central dimer reaches local equilibrium (around $\Omega t \simeq 2000$), the slow population transfer to the edge dimers leads to the establishment of a second plateau in the coherences. From the perspective of the central-to-edge dimer dynamics, a flux plateau is expected after all rapid intra-dimer transients have settled. Further, it is seen that $\operatorname{Im} \tilde{\rho}_{45}(t) \simeq \operatorname{Im} \tilde{\rho}_{32}(t)$ over these longer times, reflecting the fact that since the two central units are now equally populated, transfer to the two adjacent monomers (states φ_2 and φ_5) occurs at equal rates.

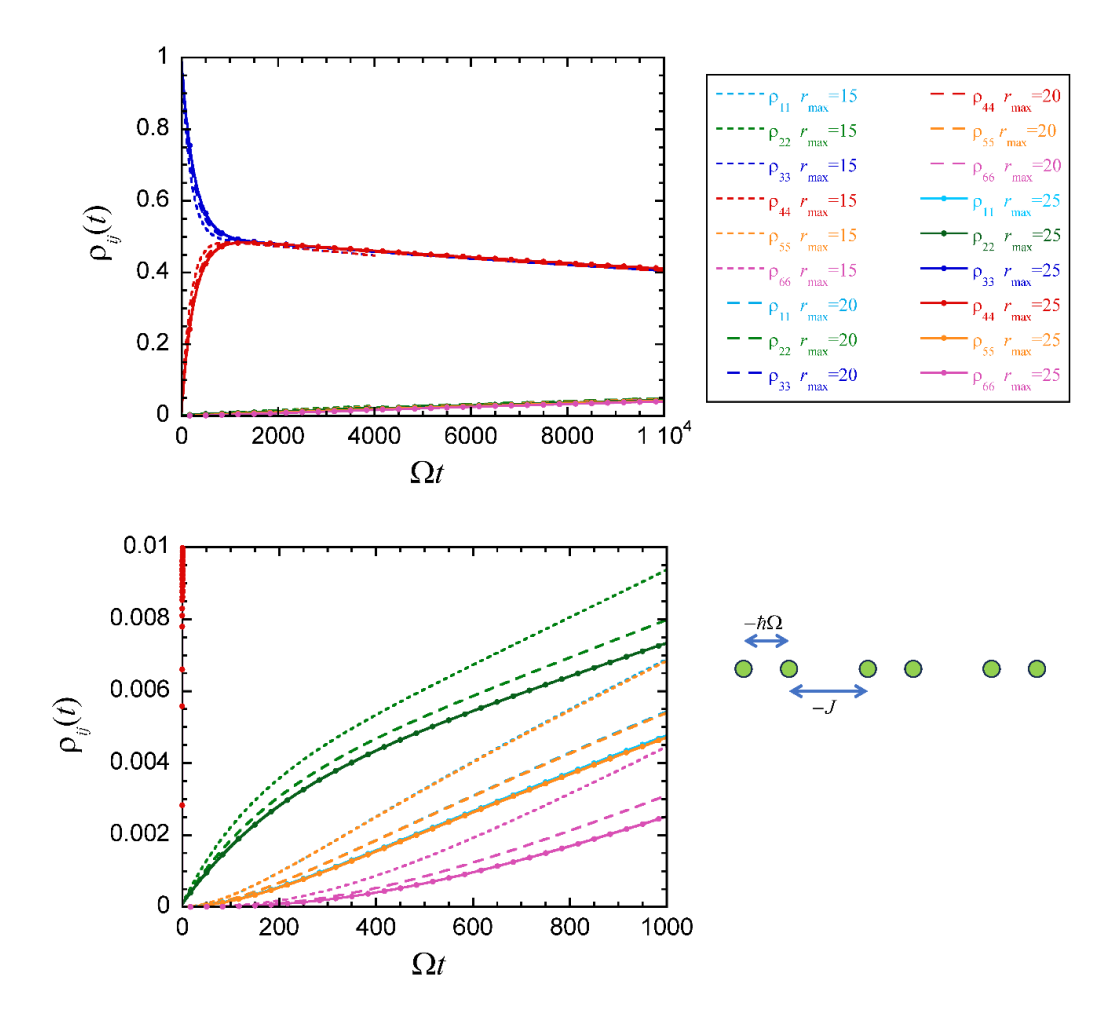


Fig. 8. Time evolution of populations for a three-dimer system with the states of the monomers coupled to Ohmic baths with parameters given in the text. The SMatPI results were obtained with $\Omega \Delta t = 0.02$ and $r_{\text{max}} = 15 - 25$ with matrices computed with the kink sum algorithm. The right panel shows the early rise of the edge dimer populations.

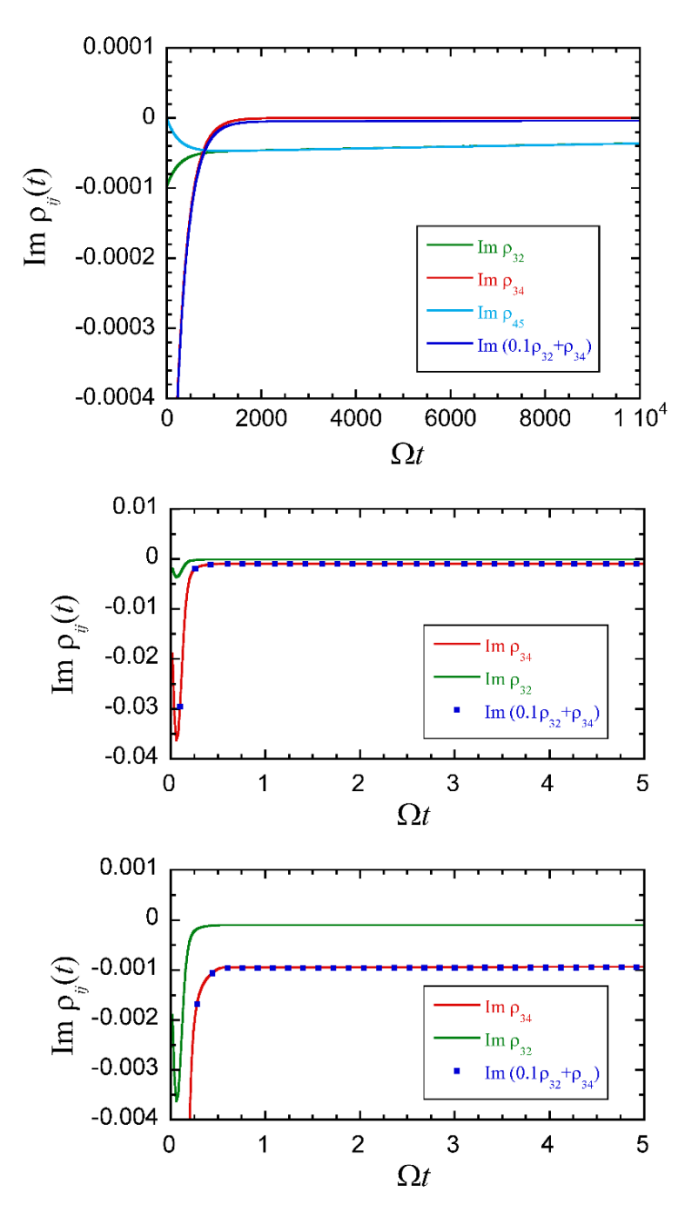


Fig. 9. Time evolution of the imaginary components of some off-diagonal elements of the RDM for the three-dimer model. The bottom panel shows early time values.

7. Discussion and concluding remarks

The kink sum algorithm presented in this paper offers an efficient method for performing the path sum in some of the most demanding situations encountered in system-bath dynamics, most notably when strong system-bath coupling induces long memory and necessitates small time steps. The efficiency of the algorithm does not rely on weakly coupled, low-frequency or high-temperature baths, offering an excellent alternative to other methods suitable for regimes characterized by strongly quantum mechanical behaviors.

In Feynman's continuous-space formulation of the real-time path integral,³⁹⁻⁴⁰ all paths contribute with the same weight. The strong dependence of path weight on path shape that is exploited in the present paper is a consequence of the finite energy range available to discrete (or DVR-discretized) Hamiltonians.

Early work on continuous systems utilized momentum⁸² and energy⁸³ filters to construct propagators with a finite spatial span. Thus, the classification of paths into fixed-amplitude equivalence classes offers new insights into the structure of the path sum for discrete systems. Further, recent work⁷⁴ has shown that this structure can be exploited in situations where the costly path sums must be performed a large number of times with different system parameters, as in the case of averaging dynamical results with respect to static disorder or including time-dependent fields.

The numerical examples presented pertain to several different types of processes, with a wide range of parameters characteristic of some of the most challenging regimes in quantum simulation. The convergence of the kink sum algorithm across all these regimes is very encouraging and complements well the already available fully quantum mechanical methods for simulating system-bath dynamics.

Acknowledgment

This material is based upon work supported by the National Science Foundation under Award CHE-1955302.

References

- 1. Beck, M. H.; Jäckle, A.; Worth, G. A.; Meyer, H.-D., The multiconfiguration time-dependent Hartree (MCTDH) method: a highly efficient algorithm for propagating wavepackets. *Phys. Rep.* **2000**, 324, 1-105.
- 2. Worth, G. A.; Meyer, H. D.; Köppel, H.; Cederbaum, L. S.; Burghardt, I., Using the MCTDH wavepacket propagation method to describe multimode non-adiabatic dynamics. *International Reviews in Physical Chemistry* **2008**, *27* (3), 569-606.
- 3. White, S. R.; Feiguin, A. E., Real-time evolution using the density matrix renormalization group. *Phys. Rev. Lett.* **2004**, *93*, 076401.
- 4. Paeckel, S.; Köhler, T.; Swoboda, A.; Manmana, S. R.; Schollwöck, U.; Hubig, C., Time-evolution methods for matrix-product states. *Annals of Physics* **2019**, *411*, 167998.
- 5. Wang, H.; Sun, X.; Miller, W. H., Semiclassical approximations for the calculation of thermal rate constants for chemical reactions in complex molecular systems. *J. Chem. Phys.* **1998**, *108*, 9726-9736.
- 6. Miller, W. H., Generalization of the linearized approximation to the semiclassical initial value representation for reactive flux correlation functions. *J. Phys. Chem.* **1999**, *103*, 9384-9387.
- 7. Wigner, E., On the Quantum Correction For Thermodynamic Equilibrium. *Physical Review* **1932**, 40 (5), 749-759.
- 8. Moyal, J. E., Quantum mechanics as a statistical theory. *Mathematical Proceedings of the Cambridge Philosophical Society* **1949**, *45* (1), 99-124.
- 9. Heller, E. J., Wigner phase space method Analysis for semiclassical applications. *J. Chem. Phys.* **1976**, *65*, 1289.
- 10. Brown, R. C.; Heller, E. J., Classical trajectory approach to photodissociation: the Wigner method. *J. Chem. Phys.* **1981**, *75*, 186.
- 11. Shao, J.; Makri, N., Forward-backward semiclassical dynamics with linear scaling. *J. Phys. Chem. A* **1999**, *103*, 9479-9486.
- 12. Liu, J., Recent advances in the linearized semiclassical initial value representation/classical Wigner model for the thermal correlation function. *International Journal of Quantum Chemistry* **2015**, *115* (11), 657-670.
- 13. Meyer, H.-D.; Miller, W. H., A classical analog for electronic degrees of freedom in nonadiabatic collision processes. *J. Chem. Phys.* **1979**, *70*, 3214-3223.
- 14. Stock, G.; Thoss, M., Semiclassical description of nonadiabatic quantum dynamics. *Phys. Rev. Lett.* **1997**, *78*, 578-581.
- 15. Liu, J., A unified theoretical framework for mapping models for the multi-state Hamiltonian. *The Journal of Chemical Physics* **2016**, *145* (20), 204105.
- 16. Liu, J.; He, X.; Wu, B., Unified Formulation of Phase Space Mapping Approaches for Nonadiabatic Quantum Dynamics. *Accounts of Chemical Research* **2021**, *54* (23), 4215-4228.
- 17. Cotton, S. J.; Miller, W. H., Symmetrical windowing for quantum states in quasi-classical trajectory simulations. *J. Phys. Chem. A* **2013**, *117*, 7190-7194.
- 18. Miller, W. H.; Cotton, S. J., Classical molecular dynamics simulation of electronically non-adiabatic processes. *Faraday Discussions* **2016**, *195* (0), 9-30.
- 19. Ehrenfest, P., Bemerkung über die angenäherte Gültigkeit der klassischen Mechanik innerhalb der Quantenmechanik. *Z. Phys.* **1927**, *45*, 455-457.
- 20. Tully, J. C., Perspective: Nonadiabatic dynamics theory. *The Journal of Chemical Physics* **2012**, 137 (22), 22A301.
- 21. Tully, J. C.; Preston, R. K., Trajectory surface hopping approach to nonadiabatic molecular collisions: the reaction of H+ with D2. *J. Chem. Phys.* **1971**, *55*, 562-572.
- Tully, J. C., Molecular dynamics with electronic transitions. J. Chem. Phys. 1990, 93, 1061-1071.
- 23. Subotnik, J. E.; Jain, A.; Landry, B.; Petit, A.; Ouyang, W.; Bellonzi, N., Understanding the Surface Hopping View of Electronic Transitions and Decoherence. *Annual Review of Physical Chemistry* **2016**, *67* (1), 387-417.

- 24. Lambert, R.; Makri, N., Quantum-classical path integral: Classical memory and weak quantum nonlocality. *J. Chem. Phys.* **2012**, *137*, 22A552.
- 25. Lambert, R.; Makri, N., Quantum-classical path integral: Numerical formulation. *J. Chem. Phys.* **2012,** *137*, 22A553.
- 26. Kapral, R.; Ciccotti, G., Mixed quantum-classical dynamics. J. Chem. Phys. 1999, 110, 8919-8929.
- 27. Kapral, R., Quantum dynamics in open quantum-classical systems. *J. Phys. Cond. Matt.* **2015,** *27*, 073201.
- 28. Cao, J.; Voth, G. A., The formulation of quantum statistical mechanics based on the Feynman path centroid density. II. Dynamical properties. *The Journal of Chemical Physics* **1994**, *100* (7), 5106-5117.
- 29. Voth, G. A., Path integral centroid methods in quantum statistical mechanics and dynamics. *Adv. Chem. Phys.* **1996**, *93*, 135.
- 30. Jang, S.; Voth, G. A., A derivation of centroid molecular dynamics and other approximate time evolution methods for path integral centroid variables. *J. Chem. Phys.* **1999**, *111*, 2371-2384.
- 31. Craig, I. R.; Manolopoulos, D. E., Quantum statistics and classical mechanics: Real time correlation functions from ring polymer molecular dynamics. *J. Chem. Phys.* **2004**, *121*, 3368-3373.
- 32. Habershon, S.; Manolopoulos, D. E.; Markland, T. E.; Miller, T. F., Ring-polymer molecular dynamics: Quantum effects in chemical dynamics from classical trajectories in an extended phase space. *Annu. Rev. Phys. Chem.* **2013**, *64*, 387-413.
- 33. Althorpe, S. C., Path-integral approximations to quantum dynamics. *The European Physical Journal B* **2021**, *94* (7), 155.
- 34. Chandler, D.; Wolynes, P. G., Exploiting the isomorphism between quantum theory and the classical statistical mechanics of polyatomic fluids. *J. Chem. Phys.* **1981**, *74*, 4078-4095.
- 35. Feynman, R. P., *Statistical Mechanics*. Addison-Wesley: Redwood City, 1972.
- 36. Caldeira, A. O.; Leggett, A. J., Path integral approach to quantum Brownian motion. *Physica A* **1983**, *121*, 587-616.
- 37. Chandler, D., *Introduction to Modern Statistical Mechanics*. Oxford University Press: New York, 1987.
- 38. Makri, N., The linear response approximation and its lowest order corrections: an influence functional approach. *J. Phys. Chem.* **1999**, *103*, 2823-2829.
- 39. Feynman, R. P., Space-time approach to non-relativistic quantum mechanics. *Rev. Mod. Phys.* **1948**, 20, 367-387.
- 40. Feynman, R. P.; Hibbs, A. R., *Quantum Mechanics and Path Integrals*. McGraw-Hill: New York, 1965.
- 41. Feynman, R. P.; Vernon, F. L., The theory of a general quantum system interacting with a linear dissipative system. *Ann. Phys.* **1963**, *24*, 118-173.
- 42. Lester Jr., W. A.; Hammond, B. L., Quantum Monte Carlo for the electronic structure of atoms and molecules. *Ann. Rev. Phys. Chem.* **1990**, *41*, 283-311.
- 43. Suzuki, M., *Quantum Monte Carlo methods in condensed matter physics*. World Scientific: Singapore, 1993.
- 44. Ceperley, D. M.; Mitas, L., Quantum Monte Carlo methods in chemistry. *Adv. Chem. Phys.* **1996**, 93, 1.
- 45. Makri, N., Improved Feynman propagators on a grid and non-adiabatic corrections within the path integral framework. *Chem. Phys. Lett.* **1992,** *193*, 435-444.
- 46. Topaler, M.; Makri, N., System-specific discrete variable representations for path integral calculations with quasi-adiabatic propagators. *Chem. Phys. Lett.* **1993**, *210*, 448.
- 47. Makri, N.; Makarov, D. E., Tensor multiplication for iterative quantum time evolution of reduced density matrices. I. Theory. *J. Chem. Phys.* **1995**, *102*, 4600-4610.
- 48. Makri, N.; Makarov, D. E., Tensor multiplication for iterative quantum time evolution of reduced density matrices. II. Numerical methodology. *J. Chem. Phys.* **1995**, *102*, 4611-4618.
- 49. Makri, N., Numerical path integral techniques for long-time quantum dynamics of dissipative systems. *J. Math. Phys.* **1995,** *36*, 2430-2456.

- 50. Ishizaki, A.; Tanimura, Y., Quantum Dynamics of System Strongly Coupled to Low-Temperature Colored Noise Bath: Reduced Hierarchy Equations Approach. *Journal of the Physics Society Japan* **2005**, 74 (12), 3131-3134.
- 51. Tanimura, Y., Numerically "exact" approach to open quantum dynamics: The hierarchical equations of motion (HEOM). *The Journal of Chemical Physics* **2020**, *153* (2), 020901.
- 52. Makri, N., Small matrix disentanglement of the path integral: overcoming the exponential tensor scaling with memory length. *J. Chem. Phys.* **2020**, *152*, 041104.
- 53. Makri, N., Small matrix path integral for system-bath dynamics. *J. Chem. Theory and Comput.* **2020,** *16*, 4038–4049.
- 54. Makri, N., Small matrix path integral with extended memory. *J. Chem. Theory and Comput.* **2021**, *17*, 1-6.
- 55. Kundu, S.; Dani, R.; Makri, N., B800-to-B850 relaxation of excitation energy in bacterial light harvesting: All-state, all-mode path integral simulations. *J. Chem. Phys.* **2022**, *157*, 115101.
- 56. Kundu, S.; Dani, R.; Makri, N., Tight inner ring architecture and quantum motion of nuclei enable efficient energy transfer in bacterial light harvesting. *Science Advances* **2022**, *8* (43), eadd0023.
- 57. May, V.; Kühn, O., Charge and Energy Transfer Dynamics in Molecular Systems. 2nd ed.; Wiley: 2008.
- 58. Hestand, N. J.; Spano, F. C., Expanded Theory of H- and J-Molecular Aggregates: The Effects of Vibronic Coupling and Intermolecular Charge Transfer. *Chemical Reviews* **2018**, *118* (15), 7069-7163.
- 59. Kundu, S.; Makri, N., Intramolecular vibrations in excitation energy transfer: Insights from real-time path integral calculations. *Annual Review of Physical Chemistry* **2022**, *73* (1), 349-375.
- 60. Makri, N., Topological aspects of system-bath Hamiltonians and a vector model for multisite systems coupled to local, correlated or common baths. *J. Chem. Phys.* **2023**, *158*, 144107.
- 61. Sim, E.; Makri, N., Tensor propagator with weight-selected paths for quantum dissipative dynamics with long-memory kernels. *Chem. Phys. Lett.* **1996**, *249*, 224-230.
- 62. Sim, E.; Makri, N., Filtered propagator functional for iterative dynamics of quantum dissipative systems. *Comp. Phys. Commun.* **1997**, *99*, 335-354.
- 63. Sim, E., Quantum dynamics for a system coupled to slow baths: on-the-fly filtered propagator method. *J. Chem. Phys.* **2001**, *115*, 4450-4456.
- 64. Lambert, R.; Makri, N., Memory path propagator matrix for long-time dissipative charge transport dynamics. *Mol. Phys.* **2012**, *110*, 1967-1975.
- 65. Makri, N., Quantum Dynamics Methods Based on the Real-Time Path Integral. In *Comprehensive Computational Chemistry (First Edition)*, Yáñez, M.; Boyd, R. J., Eds. Elsevier: Oxford, 2024; pp 293-305.
- 66. Kundu, S.; Makri, N., PathSum: A C++ and Fortran suite of fully quantum mechanical real-time path integral methods for (multi-)system + bath dynamics. *The Journal of Chemical Physics* **2023**, *158* (22).
- 67. Makri, N., Blip decomposition of the path integral: Exponential acceleration of real-time calculations for quantum dissipative systems. *J. Chem. Phys.* **2014**, *141*, 134117.
- 68. Makri, N., Exploiting classical decoherence in dissipative quantum dynamics: Memory, phonon emission, and the blip sum. *Chem. Phys. Lett.* **2014**, *593*, 93-103.
- 69. Banerjee, T.; Makri, N., Quantum-classical path integral with self-consistent solvent-driven propagators. *J. Phys. Chem.* **2013**, *117*, 13357-13366.
- 70. Walters, P. L.; Makri, N., Iterative quantum-classical path integral with dynamically consistent state hopping. *J. Chem. Phys.* **2016**, *144*, 044108.
- 71. Kundu, S.; Makri, N., Small matrix quantum-classical path integral. *J. Phys. Chem. Lett.* **2022**, *13*, 3492–3498.
- 72. Strathearn, A.; Kirton, P.; Kilda, D.; Keeling, J.; Lovett, B. W., Efficient non-Markovian quantum dynamics using time-evolving matrix product operators. *Nature Communications* **2018**, *9*, 3322.
- 73. Schollwöck, U., The density-matrix renormalization group in the age of matrix product states. *Annals of Physics* **2011**, *326*, 96-192.
- 74. Makri, N., Path integral over equivalence classes for quantum dynamics with static disorder. *The Journal of Physical Chemistry Letters* **2024**, *15* (5), 1462-1468.

- 75. Dani, R.; Makri, N., Quantum state-to-state rates for multistate processes from coherences. *The Journal of Physical Chemistry Letters* **2022**, *13* (34), 8141-8149.
- 76. Bose, A.; Makri, N., Non-equilibrium reactive flux: A unified framework for slow and fast reaction kinetics. *J. Chem. Phys.* **2017**, *147*, 152723.
- 77. Frenkel, J., On the transformation of light into heat in solids. *Phys. Rev.* **1931,** *37*, 17.
- 78. May, V.; Kühn, O., Charge and energy transfer dynamics in molecular systems. 3rd ed.; Wiley: 2011.
- 79. Schröter, M.; Ivanov, S. D.; Schulze, J.; Polyutov, S. P.; Yan, Y.; Pullerits, T.; Kühn, O., Exciton–vibrational coupling in the dynamics and spectroscopy of Frenkel excitons in molecular aggregates. *Physics Reports* **2015**, *567*, 1-78.
- 80. Leggett, A. J.; Chakravarty, S.; Dorsey, A. T.; Fisher, M. P. A.; Garg, A.; Zwerger, W., Dynamics of the dissipative two-state system. *Rev. Mod. Phys.* **1987**, *59*, 1-85.
- 81. Dani, R.; Makri, N., Time-evolving quantum superpositions in open systems and the rich content of coherence maps. *The Journal of Physical Chemistry B* **2022**, *126* (45), 9361-9375.
- 82. Makri, N., Effective non-oscillatory propagator for Feynman path integration in real time. *Chem. Phys. Lett.* **1989**, *159*, 489-498.
- 83. Makri, N., On smooth Feynman propagators for real time path integrals. *J. Phys. Chem.* **1993,** *97*, 2417-2424.